IN VITRO CHARACTERIZATION AND ASSESSMENT OF NOVEL DNA ORIGAMI-APTAMER MODIFICATION INTENDED FOR TARGETING GLIOBLASTOMA-ASSOCIATED BIOMARKER NUCLEOLIN

by

Bailey Jacob O'Shea

A Thesis
Submitted to the
Graduate Faculty
of
George Mason University
in Partial Fulfillment of
The Requirements for the Degree
of
Master of Science
Bioengineering

Committee:

_____	Dr. Rémi Veneziano, Thesis Director
_____	Dr. Shani Ross, Committee Member
_____	Dr. Barney Bishop, Committee Member
_____	Dr. Michael Buschmann, Department Chair
_____	Dr. Kenneth S. Ball, Dean, Volgenau School of Engineering
Date:_____	Summer Semester 2021 George Mason University Fairfax, VA

In Vitro Characterization and Assessment of Novel DNA Origami-Aptamer Modification Intended for Targeting Glioblastoma-Associated Biomarker Nucleolin

A Thesis submitted in partial fulfillment of the requirements for the degree of Bioengineering Master of Science at George Mason University

by

Bailey Jacob O'Shea
Bachelor of Science
George Mason University, 2020

Director: Rémi Veneziano, Assistant Professor
Department of Bioengineering

Summer Semester 2021
George Mason University
Fairfax, V

DEDICATION

This work is dedicated to my family and best friends, John O'Shea and Connor O'Shea, who have supported me throughout my academic career. They have always been there when I needed help making either school- or life-related decisions and during times of stress, I greatly appreciate it. As always, take time to relax, surround yourself by people you love and drive safe ☺.

ACKNOWLEDGEMENTS

I would like to thank my family (Connor O'Shea and John O'Shea) for the support they have provided me throughout my academic career. Also, I would like to thank my committee, Dr. Shani Ross, Dr. Barney Bishop and Dr. Remi Veneziano. I felt my committee was a well-rounded group of individuals that provided great ideation and expertise. My friends and colleagues I have made during this research including Shrishti, Esra, Leo, Shawn and Joshua; this group of people are amazing and they provided a great atmosphere when working. I first met Dr. Veneziano approximately three years ago during my 3rd year of undergrad. After seeing his field of expertise and the fascinating aspects of DNA nanotechnology, I knew that is what I to further learn. These words cannot describe how grateful I am to Dr. Veneziano for dedicating the time and effort to teach me. Additionally, an enormous appreciation to Mrs. Carol McHugh is well-deserved. Her assistance made this research process much more manageable and I greatly appreciate her effort and time.

TABLE OF CONTENTS

LIST OF TABLES

LIST OF FIGURES

LIST OF ABBREVIATIONS

Agarose Dissolving Buffer ..... ADB
Antisense Oligonucleotides ..... ASO
Asymmetric Polymerase Chain Reaction ..... aPCR
Base Pairs ..... bp
Breast Cancer ..... BC
Deoxyribonucleic Acid ..... DNA
Double-Stranded Deoxyribonucleic Acid ..... dsDNA
Doxorubicin ..... DOX
High-Fidelity ..... Hi-Fi
Human Epidermal Growth Factor Receptor 2 ..... HER2
Magnesium Chloride ..... $MgCl_2$
Magnesium Sulfate ..... $MgSO_4$
Nanoparticle ..... NP
Sodium Chloride ..... NaCl
Near-Infrared Spectroscopy ..... NIR
Nucleolin ..... NCL
Nucleoside Triphosphate ..... NTP
Photodynamic Therapy ..... PDT
Polymerase Chain Reaction ..... PCR
Prostate-Specific Membrane Antigen ..... PSMA
Ribonucleic Acid ..... RNA
Reactive Oxygen Species ..... ROS
Revolutions Per Minute ..... rpm
Single-Stranded Deoxyribonucleic Acid ..... ssDNA
Systematic Evolution of Ligands by Exponential Enrichment ..... SELEX
Tris-Acetate EDTA ..... TAE
Quantum Dot ..... QD

ABSTRACT

IN VITRO CHARACTERIZATION AND ASSESSMENT OF NOVEL DNA ORIGAMI-APTAMER MODIFICATION INTENDED FOR TARGETING GLIOBLASTOMA-ASSOCIATED BIOMARKER NUCLEOLIN

Bailey Jacob O'Shea, M.S.

George Mason University, 2021

Thesis Director: Dr. Rémi Veneziano

Ample amounts of literature have demonstrated the practicality of functionalizing DNA origami with aptamers—single-stranded DNA or RNA target-specific ligands with similar binding affinities to monoclonal antibodies—to effectively target and treat a wide range of malignancies. When functionalizing origami with aptamers, the current method relies on the use of staple strands that can be used to hybridize the aptamer of choice modified with a complementary sequence or modified with overhangs bearing the aptamer sequences. These approaches require additional steps during both the computational design and *in vitro* synthesis stage and limits our capacity of functionalization. Herein, we provide a novel technique that overcomes these additional steps while allowing for the functionalization of origami with aptamers. We demonstrate by simply designing single-stranded DNA (ssDNA) aptamer "loops", we are able to introduce aptamers at precise locations within the scaffold sequence while retaining target binding without the need to employ modified staples. Through the use of agarose

gel electrophoresis, we were able to show the characterization of two structures—a 42 bp edge 2-Dimensional triangle and 3-Dimensional tetrahedron—presenting the well-studied thrombin 29-mer and AS1411 26-mer nucleolin aptamer. After exposing thrombin to our origami-aptamer modified constructs, we observed each structure had the ability to effectively bind to thrombin. Our new sequence-aptamer functionalization technique may pave the way for simple design of readily functionalized DNA origami nanoparticles for a wide range of fields including diagnostic and therapeutic-related research.

BACKGROUND

1. Brief History of DNA Nanotechnology

Deoxyribonucleic acid, more commonly known as DNA, is one of the most well-studied molecules after being serendipitously discovered by Friedrich Miescher in 1869 [1]. DNA serves as a nanocarrier housing the genetic makeup specific to an individual. DNA consists of four unique bases—adenine (A), thymine (T), guanine (G) and cytosine (C)—linked by sugar-phosphate ester bonds, creating single stranded DNA (ssDNA). When two ssDNA have complementary bases they adopt double-stranded helical duplex structure maintained via A-T and G-C Watson-Crick binding [2], [3]. It was not until the 1980s that Nadrian Seeman exploited the specific biochemical feature and leveraged the Watson-Crick base pairing mechanism to control the assembly of multiple strands with complementary sequence and program the assembly of 2-D and 3-D structures [4], [5]. As this interdisciplinary field began to experience more recognition due to its potential, discoveries detailing novel methods for formulating DNA-based nanoparticles (NPs) started to emerge. Notably, in 2006, Paul Rothemund established the next advancement in DNA nanotechnology developing the DNA origami technology [6]. DNA origami relies on annealing a plurality of small ssDNA staple strands onto a long ssDNA scaffold, typically the M13 bacteriophage genome, to create nearly any arbitrary one-, two- or three-dimensional (1-D, 2-D and 3-D) structures. The strict Watson-Crick bp rule

allowed Rothemund to systematically control the hybridization of staple strands at precise locations on the DNA scaffold. As a result, researchers began to assess the functionalization potential of DNA origami through the attachment of various organic and inorganic molecules [7], [8].

Nearly a decade after Seeman's discovery (1990s), functional nucleic acids (FNAs) such as aptamers and DNAzymes were introduced as potential alternatives to antibodies and enzymes, respectively, due to their favorable low cost and high purity properties. Established by Tuerk and Gold in 1990, aptamers or "chemical antibodies" are synthetic ssDNA or RNA ligands that present high affinity and target-specific capabilities resulting from the systematic evolution of ligands by exponential enrichment (SELEX) process [9]. Compared to monoclonal antibodies, aptamers appear to be superior as a result from their biocompatibility, low cost, *in vitro* synthesis, high affinity and specificity [10]. Discovered by Breaker and Joyce, DNAzymes or deoxyribozymes are synthetic ssDNA molecules with catalytic capabilities to cleave RNA molecules [11]. Stability and inexpensive cost of production are two of the major benefits that accompany DNAzymes.

1.1 Aptamers

As previously emphasized, aptamers are ssDNA or RNA molecules with high affinity and biomarker-specific targeting capabilities as a result from the cyclic SELEX process (**Fig. 1**) [9], [12] . This process initiates with the incubation of an ideal target protein into a large pool of free-floating nucleic acids. Where unbound-target sequences are retained, bounded sequences are amplified via polymerase chain reaction (PCR). The

mechanism by which aptamers bind to their targets relies on a key-to-lock relationship; meaning, in the presence of a biomarker target, the aptamer folds into a 3-D structure expressing a shape complementary to the target binding site (**Fig 2**). Having the ability to be used to functionalized organic and inorganic NPs that can serve as drug nanocarriers, the aptamers become a targeting moieties of choice that can be tailored to a wide range of applications.

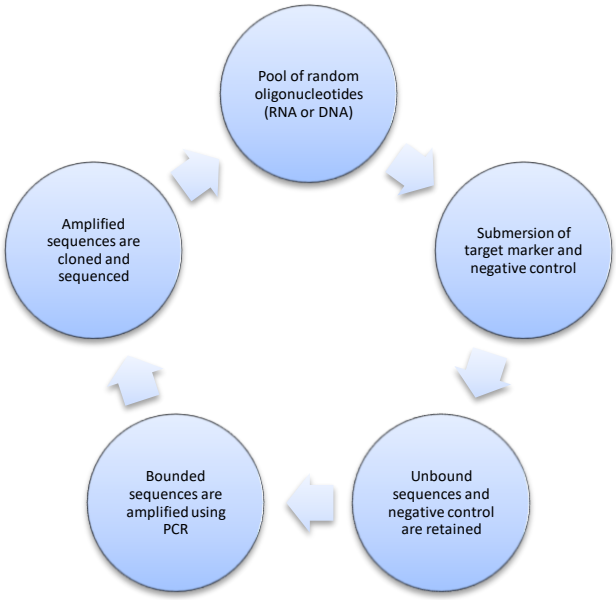

Figure 1: Schematic illustrating the cyclic SELEX process for the production of aptamers. The initial step relies on the submersion of a selected biomarker target within a large pool of random RNA or DNA nucleic acids, aptamer-type dependent. After sufficient time of target exposure, unbound sequences and negative control are retained.

Those target-bound sequences are amplified using PCR, cloned and sequenced for characterization. This process is repeated until the purity of the aptamer is satisfactory.

With target-specific and functionalization capabilities, aptamers are being exposed to cancer-related theranostics [13] – [17], therapeutics [18] – [20], diagnostics [21] – [23] and cellular imaging [24]. For example, Farokhzad and colleagues designed RNA aptamer-polymer (PLA-PEG-COOH) bioconjugates as nanocarriers for delivery of rhodamine-labeled dextran to prostate LNCaP epithelial cells by targeting prostate-specific membrane antigen (PSMA); compared to the control (PSMA-negative PC3 cells), the bioconjugates expressed a 77-fold increase in binding and overall better cellular uptake [13]. Similarly, Chu and researchers synthesized RNA aptamer-gelonin (anticancer phytocompound) NPs and reported a 600-fold increase in potency for PSMA-bearing cells and decreased PC3 cytotoxicity [14]. The RNA aptamer complexes discussed above shows promise in targeting efficiency and drug delivery to PSMA-expressed cells; however, follow-up *in vivo* studies assessing bioavailability and stability needs to be accomplished to further understand the practicality of these NPs.

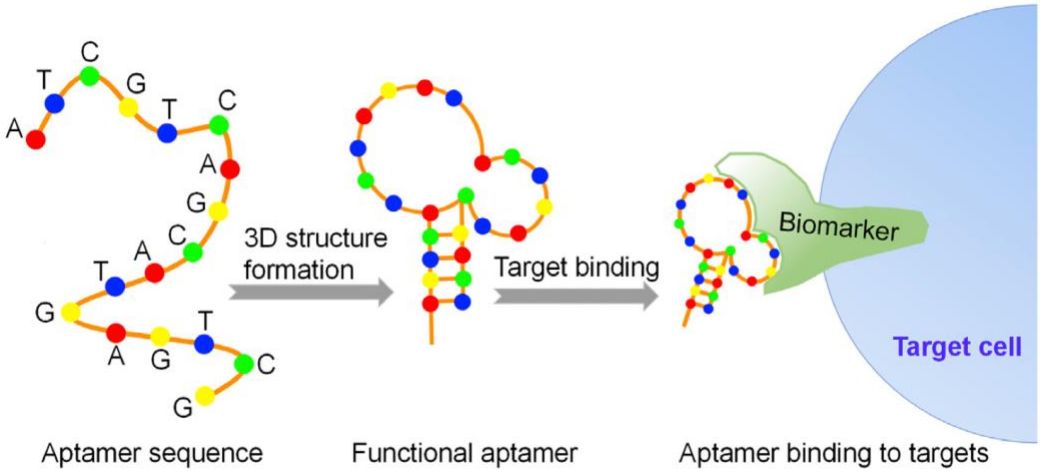

Figure 2: Schematic demonstrating the folding of an ssDNA aptamer in the presence of the target protein (biomarker). Figure from [25].

With respect to targeting a biomarker associated with various malignancies, the human epithelial growth factor receptor 2 (HER2) biomarker appears to be a well-qualified candidate considering its expression in bladder, breast, gastric, cervical, ovarian and lung cancers [26]. Taking this into consideration, Liu and researchers have utilized the SELEX process to synthesize HER2-specific DNA aptamers to effectively target and deliver doxorubicin (dox) to HER2-positive breast cancer cells. Yang et al. designed aptamer-gold NP-hybridized graphene oxide (Apt-AuNP-GO) sheets for targeting and treating MUC1-expressed breast cancer cells by means of near-infrared (NIR) light-activatable photothermal therapy [20].

Aptamer-inorganic NP functionalization has the potential to enhance properties within diagnostics and cellular imaging [21], [24]. Herr and researchers developed a rapid and reliable method for the accumulation and detection of CCRF-CEM acute leukemia cells using two separate aptamer-NPs: (1) aptamer-modified iron oxide NPs for extraction and (2) aptamer-modified fluorescent NPs for detection [21]. Further discussing the topic, Bagalkot and associates synthesized quantum dot-aptamer-dox conjugates to effectively image, treat and sense PSMA-expressed cancer cells [24].

As aptamer-related research grows, scientists and engineers may begin to synthesize target-specific ssDNA or RNA for the intention to interact with biological signaling and growth pathways. One of the most popular aptamers in cancer-related research is AS1411, formally known as AGRO100. Discovered by Aptamera (Louisville, KY), AS1411 is a 26-mer guanine-rich DNA aptamer that forms a G-quadruplex in the presence of its target protein nucleolin (NCL) [27]. In normal cells, NCL is localized in the nucleus, however, for malignant cells, NCL is overly expressed throughout the cell, including the cytoplasm, cellular membrane and nucleus, while appearing to influence carcinogenesis and proliferation [28], [29]. Therefore, AS1411-NCL binding has the potential to influence cellular pathways that regulate proliferation and carcinogenesis [15], [30] – [32]. The mechanism by which AS1411-NCL binding expresses antiproliferation properties appears to be two-fold: (1) *bcl*-2 mRNA instability leading to apoptosis [32] and (2) sustained Rac1 activation leading to methuosis (**Fig. 3**) [33]. Interestingly, Reyes-Reyes and researchers initially proposed AS1411 cellular uptake was influenced by NCL-mediated endocytosis but later emphasized it was related to

macropinocytosis, a mechanism exploited by cancer cells for rapid nutrient transportation; it appears AS1411 is initially transported into the cytoplasm via macropinocytosis and binding of AS1411 to NCL in the cytoplasm causes hyperstimulation of macropinocytosis via sustained Rac1 activation, thus increasing AS1411 cellular uptake [34]. While all studies acknowledge NCL is the binding target for AS1411, the pathway to cell death appears to be controversial and requires further elucidation; however, the AS1411 cell death pathway may relate to current active role of NCL, which may be dependent on cancer-type and/or stage.

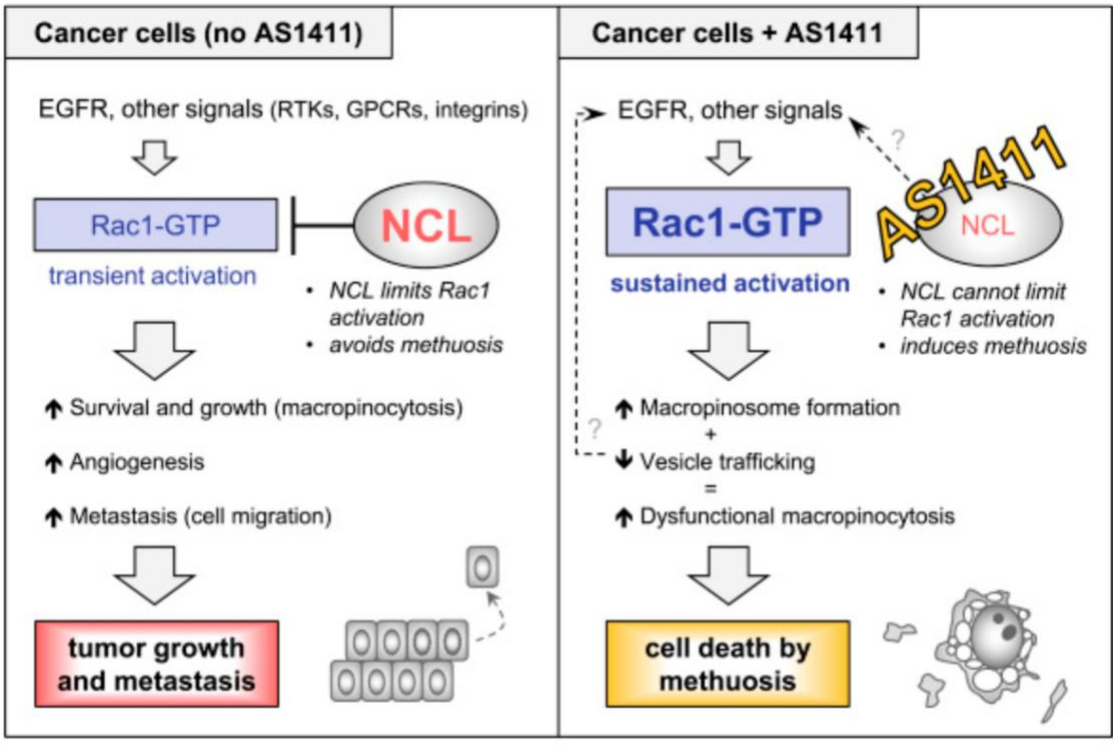

Figure 3: Schematic illustrating the methuosis pathway influenced by AS1411-Nucleolin (NCL) binding. The left panel emphasizes the regulatory properties NCL expresses in the absence of AS1411. The right panel highlights the cascading effect of AS1411-NCL binding as it influences endosomal formation. Figure from [33].

As AS1411 cancer-related applications report positive results, the future of AS1411 may entail clinical applications [15], [31], [33], [34]. Soundararajan and colleagues assessed AS1411's antiproliferation capability in adenocarcinoma MCF-7 and MDA-MB-321 breast cancer (BC) cells and MCF-10A normal mammary epithelial cells (control) to report at select concentrations, the aptamer appeared to inhibit BC growth by competing with *bcl*-2 mRNA for NCL binding; as a result, the half-life of *bcl*-2 mRNA decreased [15]. For targeting certain cancers, obstacles such as overcoming the blood brain barrier (BBB) to treat glioblastomas has forced researchers to design unique AS1411-NP conjugates that utilize BBB-favored molecules (e.g., hydrophobic lipid-soluble particles) [31].

1.2 DNA Origami

Paul Rothemund demonstrated in 2006 that discrete monodisperse DNA nanoparticles with high structural stability could be obtained by annealing short ssDNA (i.e. staple strands) with a long ssDNA scaffold (typically the M13mp18 ssDNA circular genome). With this method one can design arbitrary one-, two- and three-dimensional (1-D, 2-D and 3-D) DNA origami structures (**Fig. 4**) [6]. To this day, researchers have been able to design unique origami geometries for a wide range of cancer-related applications

including drug delivery [35] – [38], photodynamic therapy (PDT) [39], theranostics [40] and cellular imaging [41], [42].

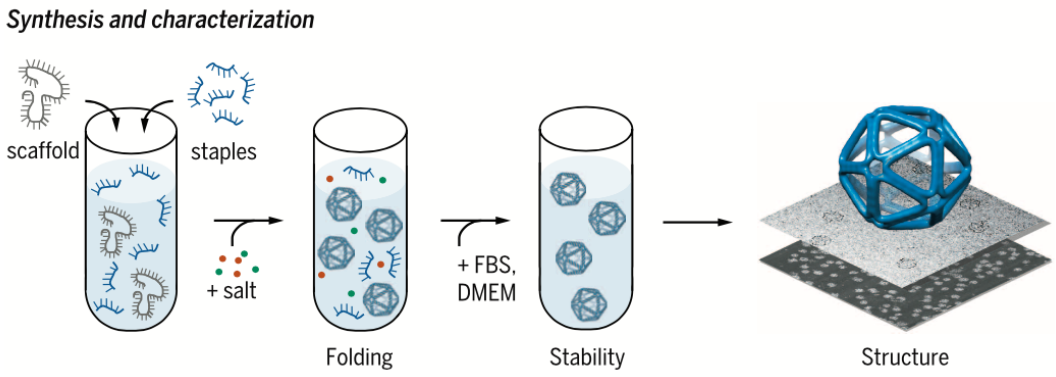

Figure 4: Synthesis and characterization of the DNA origami nanoparticles. Schematic presented by Veneziano et al. illustrating the process of annealing ssDNA scaffold with staple stands into arbitrary DNA origami shapes and stability assessment via serum (e.g., FBS and DMEM). Figure from [41].

For example, Jiang and researchers synthesized triangular-shaped and 3D tubular DNA origami structures intercalated with dox to target MCF-7 drug-sensitive and drug-resistant phenotypes; compared to free dox and dox-loaded dsDNA, which appeared to be not effectively inducing cell death, the dox-loaded origami NPs achieved cell death at the similar concentration [35]. Loaded at fixed dox concentrations, confocal fluorescence images revealed dox-loaded origami structures expressed significantly higher amounts of

intracellular dox concentration compared to free dox, suggesting cellular uptake of dox-loaded NPs may be size- and/or shape-dependent.

Being one of the first researchers to assess *in vivo* DNA origami as a drug delivery vehicle on tumor-bearing nude mice, Zhang and colleagues designed three dox-loaded origami structures (triangle, square and tube) to measure shape-related origami biodistribution and cytotoxicity (**Fig. 5**) [37]; compared to free-floating quantum dots (QDs) and QD-M13 DNA, the mice administered with QD-origami structures revealed significantly shorter elimination rates and higher light intensities at the tumor site (triangle being significantly different from the square and tube origami). At 24 hr post-QD administration, an *ex vivo* analysis revealing the accumulation, if any, of each group within the tumor and several organs (brain, heart, lung, kidney, spleen and liver); the triangular DNA origami expressed the highest and one of the lowest levels of tumor and organ accumulation, respectively. Acknowledging cellular uptake of molecules in tumor cells differ from normal cells based on the molecules size and/or shape [43], the accumulation and delivery of dox-loaded DNA origami structures in tumor-bearing nude mice appear to favor triangular-shaped DNA origami.

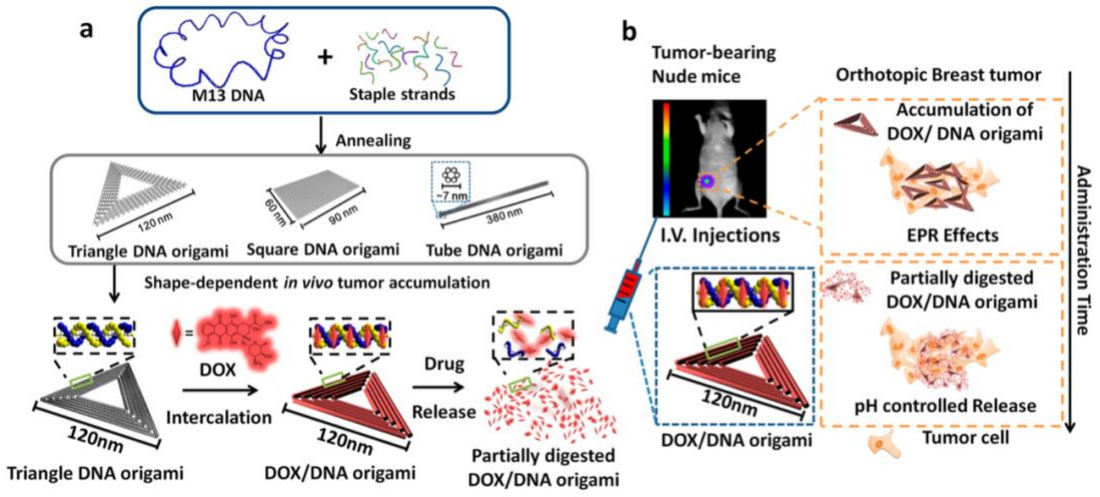

Figure 5: Schematic presented by Zhang et al. providing an overview of the DNA origami and related parameters. (a) Illustrating the process from synthesizing three (triangle, square and tube) DNA origami structures to intercalation and release of doxorubicin (dox) via digestion; (b) I.V. Injections of the dox-loaded DNA origami NPs administered in the tail and accumulation of the NPs appear to be shape-dependent and dox release regulated by intracellular pH levels. Figure from [37].

Presenting to be an effective cancer treatment, photodynamic therapy (PDT) relies on the use of ultraviolet light-photosensitizer activation for the production of highly reactive oxygen species (ROS) to induce cell death mechanisms [44] – [46]; however, the challenge appears when selectively targeting cells that lowers cytotoxicity in normal cells. By designing shape and size-dependent photosensitizer-loaded DNA origami nanoparticles, researchers may effectively transport photosensitizers to dominantly produce ROS in malignant cells [39]. Zhuang and associates synthesized BMEPC

(photosensitizer)-loaded DNA origami triangular NPs to treat *in vitro* MCF-7 cells via one- and two-photon PDT. Pre- and post-irradiation fluorescence emission was noted. With respect to one-photon irradiation, BMEPC-loaded DNA origami and free-floating BMEPC revealed cell death capabilities; however, BMEPC-loaded DNA origami expressed significantly less irradiation time and time leading to apoptosis. Using two-photon irradiation, the results were similar (halved) with respect to BMEPC-loaded DNA origami performing overall better. The authors acknowledged that DNA origami expresses limited targeting functionality, however, by integrating aptamers as part of the origami structure, this challenge may be resolved.

2. DNA Origami-Aptamer Conjugates

In the past two decades, DNA nanotechnology has experienced a great deal of attention, particularly related to the functionalization of DNA origami with targeting moieties [47], [48]. Through precise spatial attachment of aptamers on origami structures, improvements have been made regarding specific targeting capabilities [49] – [55]. Tian and researchers synthesized anticancer metal-loaded tetrahedron DNA origami functionalized with two cancer-targeting aptamers (MUC-1 and AS1411) to effectively target and treat glioma cells [51]. Moreover, Liu, Xu and Liu spatially distributed AS1411 onto cuboid DNA origami to measure its impact on cell binding and uptake in human cervical cancer (HeLa) and MCF-7 cells (**Fig. 6**) [52]. After two hours of incubation in HeLa cells, confocal microscopy images suggest that cellular uptake is dependent on the spatial distribution of AS1411, particularly favoring structure 2A. Compared to MCF-7 cells expressing less surface NCL, there appears to be little to no

significant difference in cellular uptake across the four groups with the exception of 4A (higher) and 4B. Interestingly, the authors also reported that 4A expressed the highest free-floating NCL capture efficiency rate, followed by 4B, 2A and 2B (each being significantly different from each other). Therefore, with respect to cellular uptake and binding, the orientation of AS1411 appears to be dependent on cell-type as it relates to NCL surface-level expression.

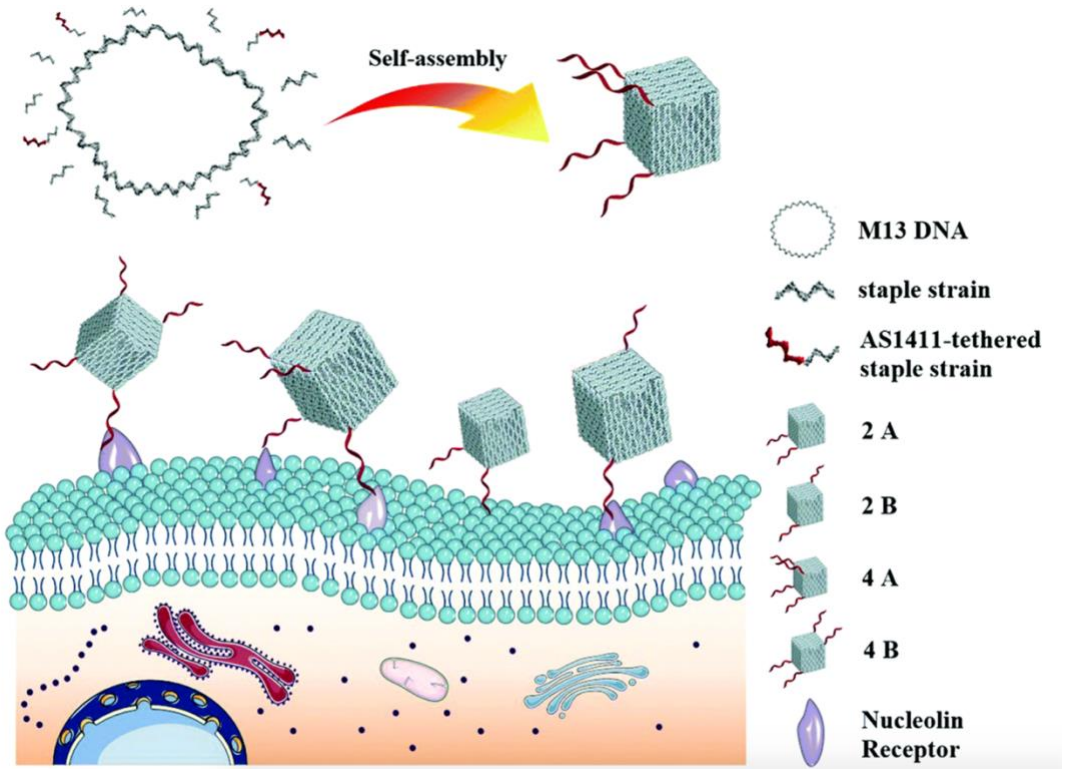

Figure 6: Spatial distribution of AS111 onto nanocubes. Schematic presented by Liu, Xu and Liu illustrating the DNA origami folding technique using the M13 scaffold and staple strands while emphasizing four unique spatially distributed AS1411-cuboid origami structures and its target biomarker (nucleolin). Figure from [52].

Moreover, Pan et al. designed a MUC1 aptamer and two antisense oligonucleotides (ASOs) planar DNA origami-based system loaded with dox to suppress gene encoding mRNA protein activity, similar to AS1411 [53]. The multi-functional origami complex served to release dox and ASOs in HeLa/Adriamycin cells. While the report revealed the dox-DNA origami-ASO group expressed overall higher cellular uptake compared to free-floating ASOs, the aptamer-embedded origami complex indicated noticeably higher cellular intensity levels, allowing for overall better cytoplasmic and nuclear exposure of dox and ASOs.

While there is an abundant amount of literature demonstrating the success and practicality of aptamer-DNA origami in cancer-related research, discoveries and challenges still remain [56] – [59]. With respect to the previously discussed applications, a common theme was observed with regards to the methodology of attaching aptamers to DNA origami; it was tailored to the staple strands via overhangs that expressed complementary bases to the aptamers. To our knowledge, no attempts have been made to functionalize DNA origami scaffold with aptamers by means of modifying the DNA sequences to include functional nucleic acid sequences.

SIGNIFICANCE

By presenting a novel DNA origami-aptamer modification method, this discovery offers three innovative and potentially groundbreaking components: (1) provide computational models that adequately design and characterize unique origami-aptamer modifications, (2) present rapid and reliable *in vitro* assays for this novel DNA origami-aptamer modification and (3) better understand origami-aptamer formulation for optimal targeting and efficiency. Based off ideal properties associated with cancer-related therapeutic agents, origami-aptamer complexes expressing this method of modification could be a great addition to the existing arsenal of treatment tools.

HYPOTHESIS

We hypothesize that modeling DNA origami scaffolds to include aptamer "loops" can simplify the design of functionalized DNA origami and precisely control the aptamer orientation and location while preserving the ability to express target binding. Here we plan to demonstrate this novel aptamer presentation technique with two unique structures: 42 bp edge 2-D triangle and 3-D tetrahedron.

SPECIFIC AIMS

Specific Aim 1: Design and Preparation of scaffold for 2-D Triangle and 3-D Tetrahedron DNA Origami Nanoparticles with Aptamer-Modified Sequence.

1. Introduction

DNA origami design and characterization are fundamental steps in synthesizing nanoparticles; these parameters are crucial to understand when functionalizing aptamer sequences with DNA origami. Herein, we aim to provide the design and characterization methodology and results pertaining to 2-D triangle and 3-D tetrahedron DNA origami-aptamer conjugates.

2. Methodology

2.1 Computational Modeling

DNA editing software (i.e., DAEDALUS [41] and Tiamat [60]) were used to model 2-D and 3-D origami-aptamer nanostructures. The geometries of interest include a 2-D 42 bp edge triangle and 3-D 42 bp edge tetrahedron, each displaying aptamers as part of its sequences. Aptamer representation in the sequences will appear as custom nucleic acid loops, signified as an 'X' in the exported scaffold sequence (Table 1). Using National Center for Biotechnology Information's (NCBI) Basic Local Alignment Search Tool (BLAST), we searched for regions of complementary between sequences. Using this tool, staple strands should not form base pairs with the aptamer sequence,

theoretically allowing the aptamer sequence to retains its 3-D target-binding shape after folding and avoiding misfolding of the nanostructures.

Herein, we aim to observe aptamer-sequence integration via two ways: (1) being part of a smaller set of sequences attached with one strand and (2) multiple incorporation along a long ssDNA origami scaffold. A 2-D triangle Tiamat model will randomly generate sequences to serve as the sequences of interest. A 522 b.p. gBlock gene fragment shown to be aPCR-capable will utilized as the tetrahedron scaffold sequence [61]. Once the gBlock sequence is imported into the model and staple strands are generated, we will design the structure to expresses aptamer loops and proper origami characteristics (i.e., staple nicks, scaffold and staple crossovers, etc.). A 42 bp edge tetrahedron map provided by DAEDALUS will be utilized when ensuring said characteristics to ensure proper folding.

2.2 Aptamer-gBlock Editing

Custom dsDNA gene fragments (gBlocks) will include one, two and three aptamer sequences at precise locations within the gBlock (Table 1). Serving as a proof of principle, gBlock gene fragments will initially include the well-known thrombin 29-mer aptamer sequence to be assessed for efficient aPCR amplification and thrombin binding after folding of the nanostructures with the amplified scaffold. Once amplification and binding is observed with the thrombin 29-mer gBlock, we aim to replace the 29-mer with the AS1411 26-mer sequence and evaluate the binding parameters.

Table 1: Table illustrating the exported 42 bp edge triangle and tetrahedron Tiamat sequences with thrombin 29-mer (red). Location of the aptamer "loops", signified by the "X", within the tetrahedron scaffold sequence.

42 bp Triangle Sequences (5' – 3') with Three Thrombin 29-mer:
ACGGCTCTTTTTTAGTCAACCCTACTTGAAGACACCGCAATCCATA
AGTAGGGTTGACTAAGAGCCGTTAGATGCGAGTCCGTGGTAGGGCAGGTTGGGGTGACTTCGCTGTACTAA
TTTCGGAGGTTCTCTAACTAGTATGGATTAGTCCGTGGTAGGGCAGGTTGGGGTGACTGCGGTGTCTTCA
CTAGTTATTTTGAGAACCTCCGAAAATGCTGGTACCATTTTCTAA
TCTCGACGTTTTGTCTGTCGACAACTATTAGTACAGCGACGCATCTA
TAGTTGTCGACAGACCGTCGAGATTAGAAAAAGTCCGTGGTAGGGCAGGTTGGGGTGACTTGGTACCAGCAT
42 bp Tetrahedron Sequences with One Thrombin 29-mer:
Scaffold (5' – 3') GGACGCTATCCAGTCTAAACATTTTACTATTACCCCCTCTGGCAAAACTTCT TTTGCAAAAGCCTCTCGCTATTTTGGTTTTTATCGTCGTCTGGTAAACGAGG GTTATGATAGTGTTGCTCTTACTATGCCTCGTAATTCCTTTTGGCGTTATGTA TCTGCATTAGTTGAATGTGGTATTCCTAAATCTCAACTGATGAATCTTTCTAC

CTGTAATAATGTTGTTCCGTTAGTTCGTTTTATTAACGTAGATTTAGTCCGTG GTAGGGCAGGTTGGGGTGACTTTCTTCCCAACGTCCTGACTGGTATAATGAG CCAGTTCTTAAXXXAATCGCATAAGGTAATTCACAATGATTAAAGTTGAAA TTAAAXXXCCATCTCAAGCCCAATTTACTACTCGTTCTGGTGTTTCTCGTCA GGGCAAGCCTTATTCACTGAATGAGCAGCTTTGTTACGTTGATTTGGGTAAT GAATATCCGGTTCTTGTCAAGATTACTCTTGATGAAGGTCAGCCAGCCTATG CGCCTGGTCTGTACACC
Staple-Strands (5’ – 3’)
CAAAAGGATTATGCGATTTTAAGAACTGGAGATAAATAACGC
GACCAGGCGCATTTTTTAGGCTGGCTCTTTAATCATTTTTTTGTGAATTACCA TTACGAGGCATTTTTTAGTAAGAGC
AACCCTCGTTCTGGATAGCGTCCGGTGTACAAACACTATCAT
TCAAGAGTAATCTCTTGAGATGGTTTAATTTCAAGACCTTCA
CAGAACGAGTATTTTTGTAAATTGGGTGACAAGAACCTTTTTGGATATTCAT AGTGAATAAGGTTTTTCTTGCCCTGA
GCTCATTCTACCCAAATCAACGTAGAGGGTGCCAACAAAGCT
AAAACGAATTGGGAAGAAAAATCTAACACCGAGAACGTTAAT
CTCATTATACCTTTTTAGTCAGGACGCTAACGGAACATTTTTTACATTATTAC AATACCACATTTTTTTCAACTAATGC
GATTTAGGAGGTAGAAAGATTCAAGCGAGAAAATTCAGTTGA
GGTAATAGTAATTTTTAATGTTTAGATACCAGACGACTTTTTGATAAAAACC

AGGCTTTTGCATTTTTAAAGAAGTTT

2.3 Asymmetric Polymerase Chain Reaction

Asymmetric polymerase chain reaction (aPCR) is a modified version of PCR that relies on the use of one primer in excess. Here we use primers with an excess of the forward primer (5': GGACGCTATCCAGTCTAAACAT) and a limited amount of the reverse primer (3': GAAAGAGGACAGATGAACGGTG) to selectively amplify thrombin-gBlock ssDNA. Forward and reverse primer concentration are 50 μM and 1 μM (50:1 ratio), respectively. The remaining elements include Ultra-purified distilled water, Hi-fi PCR buffer 10x 1.25 mL, 50 mM $MgSO_4$, 10 mM nucleoside triphosphate (NTP), DNA gBlock-thrombin/AS1411 template and *Taq* polymerase enzyme. The reaction is performed in 50 μL aPCR solution per tube. With respect to the tetrahedron gBlock-aptamer sequence, samples will be amplified using a Bio-Rad T100 Thermal Cycler programed with a Hi-Fi PCR protocol: initial heating at 94° C for 60 seconds, denaturation at 94° C for 20 seconds, primer annealing at 55° C for 30-60 seconds and amplification at 68° C for 45 seconds (enzyme-dependent: 1 minute per 1k bp for *Taq*); this cycle will be repeated 35 times and stored at 4° C until ready for post-aPCR agarose gel electrophoresis.

2.4 Agarose Gel Preparation and Electrophoresis

Agarose gels will be prepared using 1x Tris-acetate EDTA (TAE) buffer and 1.5 percent agarose at 1.5 g per 100 mL TAE. After the agarose powder is fully dissolved and

cooled, 10 mg/mL ethidium bromide is added and thoroughly mixed. The solution will be poured into a cast holding a well comb and placed at room temperature until gel formation is successful. Once formation occurs, the gel is carefully placed and submersed into an electrophoresis 1x TAE bath. Next, 10 μL of purple 6x Gel Loading dye is added per 50 μL of aPCR product. A 1kb plus DNA ladder reference will be loaded to estimate the size of aPCR dsDNA and ssDNA. The gel will be ran approximately for one hour at 90 volts to ensure separation of dsDNA and ssDNA products.

2.5 Single-Stranded DNA Purification

DNA purification will begin once the ssDNA has migrated enough in the gel to be separated from other biproducts (e.g., dsDNA) and extracted. The ssDNA is cut from the agarose gel and placed into a 15 mL tube. Agarose dissolving buffer (ADB) is poured into the tube until the gel is submersed. Once the gel has dissolved fully, we will utilize Zymo-Spin columns and collection tubes to extract gBlock-aptamer ssDNA. In increments of 740 μL, we will load the ssDNA-ADB solution into the Zymo-Spin column and centrifuge at 11k revolutions per minute (rpm) for 30 seconds. After the sample collected into the collection tube is disposed, this step is repeated until the entire ssDNA-ADB solution has experienced centrifugation. To ensure the column is dry, the final load experiences 11k rpm for 60 seconds. Next, 250 μL DNA Wash Buffer is added to each Zymo-Spin column and centrifuged at 11k rpm for 60 seconds; this step is repeated once more to ensure the purity of the sample. Lastly, 10 μL DNA Elution Buffer is carefully added to each column and once more centrifuged at 11k rpm for 60 seconds; prior to introducing the DNA Elution Buffer, collection tubes are replaced to ensure

minimal cross contamination. Lastly, the gBlock-aptamer ssDNA will be extracted and its concentration measured using a Nanodrop.

3. Results and Discussion

3.1 Two-Dimensional (2-D) Thrombin-gBlock Triangle

A 2-D thrombin-gBlock triangle model was exported from Tiamat displaying structure features including aptamer loops, loop location and orientation, sequence nicks, and base pair distance between the loops and nicks (**Fig. 7**). Loops were placed at least eight bp from the nearest sequence nick to ensure structural stability (**Fig. 8**). This placement allowed for roughly the same distance between aptamers, however, this distance may change based on the aptamer's flexibility *in vitro*. By selecting a sequence of interest (e.g., sequence 2 of the Tiamat model), we were able to observe and editing various characteristics such as sequence length and nucleic acid composition to include the sequences displayed in Table 1.

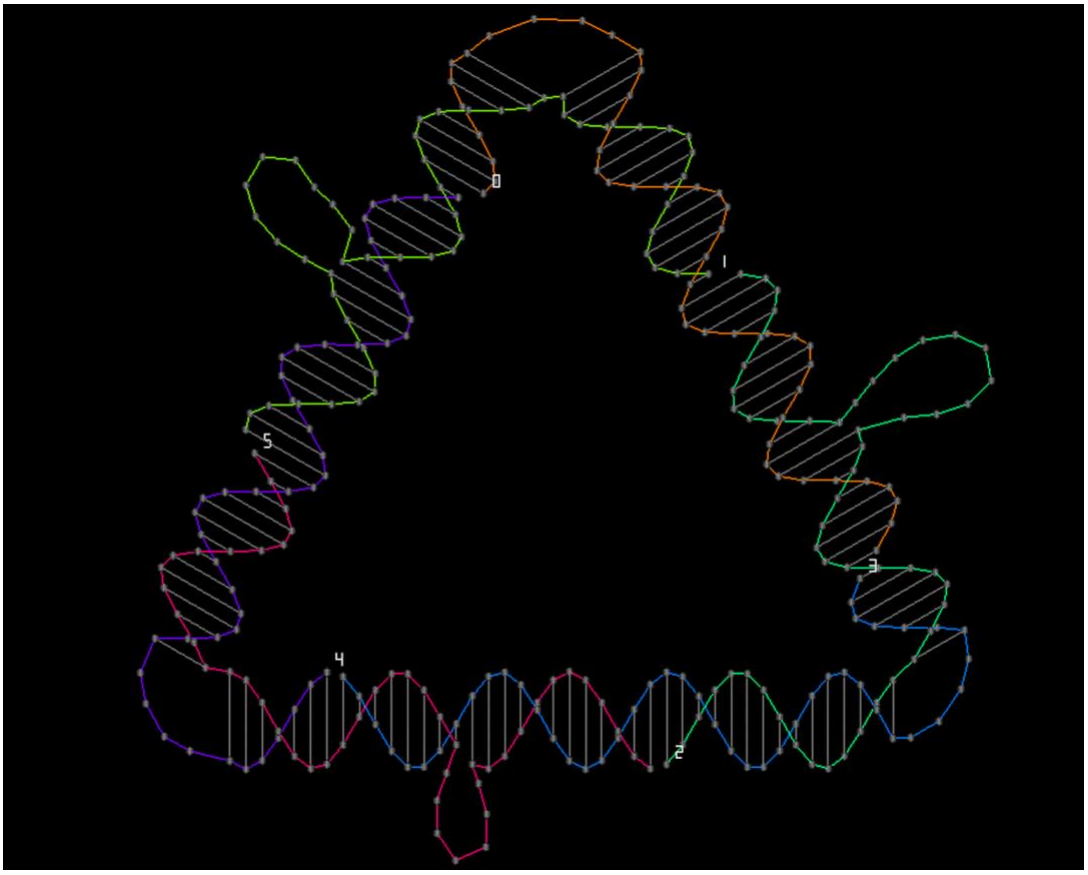

Figure 7: Exported Tiamat file of the 42 bp triangle-aptamer loop design. This schematic illustrates the precise location and orientation of aptamer loops and emphasizes loop placement from sequence nicks.

By indicating the importance of structural features (i.e., distance between aptamer loops and staple nicks) when functionalizing DNA origami with aptamer sequences, the transition of the thrombin 29-mer onto the tetrahedron remains virtually the same; however, with 3-D structures like the tetrahedron there are additional features that need to be taken into consideration when designing: distance from scaffold nick, staple nicks, scaffold crossovers and staple crossovers.

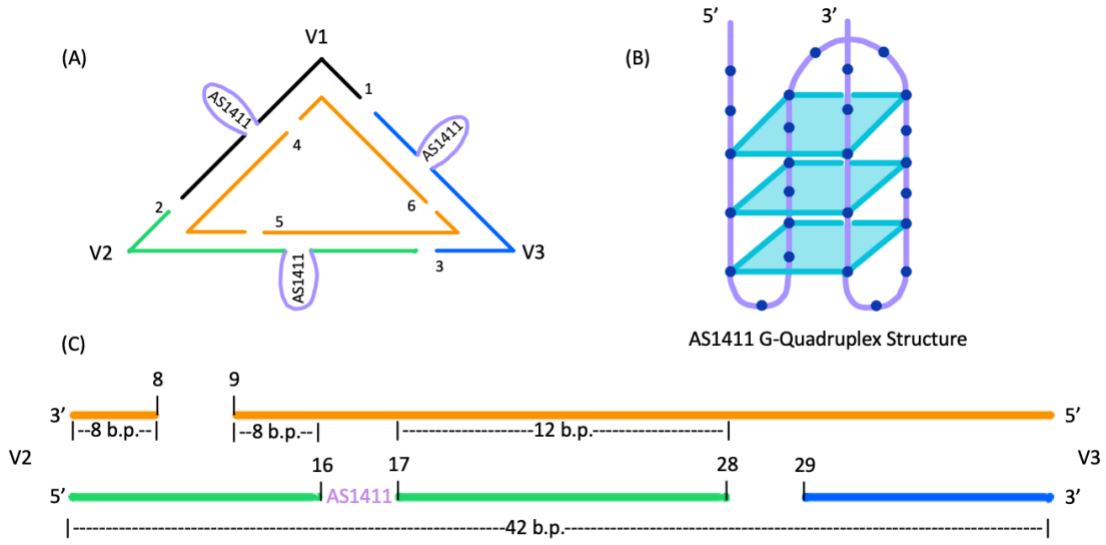

Figure 8: Schematic illustrating AS1411-DNA Origami modification. (A) Model highlighting triangular DNA origami with AS1411 modification while emphasizing the number of strands; (B) the AS1411 G-quadruplex structure; and (C) detailed base pair distancing of V2-V3 edge.

3.2 Three-Dimensional (3-D) Thrombin-gBlock Tetrahedron

Through the use of DAEDALUS, we were able to render 3-D tetrahedron and spatially place thrombin 29-mer at locations we anticipate after the DNA origami folding process (**Fig. 9**). In the model, the thrombin 29-mers were unattached from the scaffold sequence, allowing for appropriate spatial adjustment. As this model may not represent the actual tetrahedron design, it delivers a favorable visual aid in 3-D space.

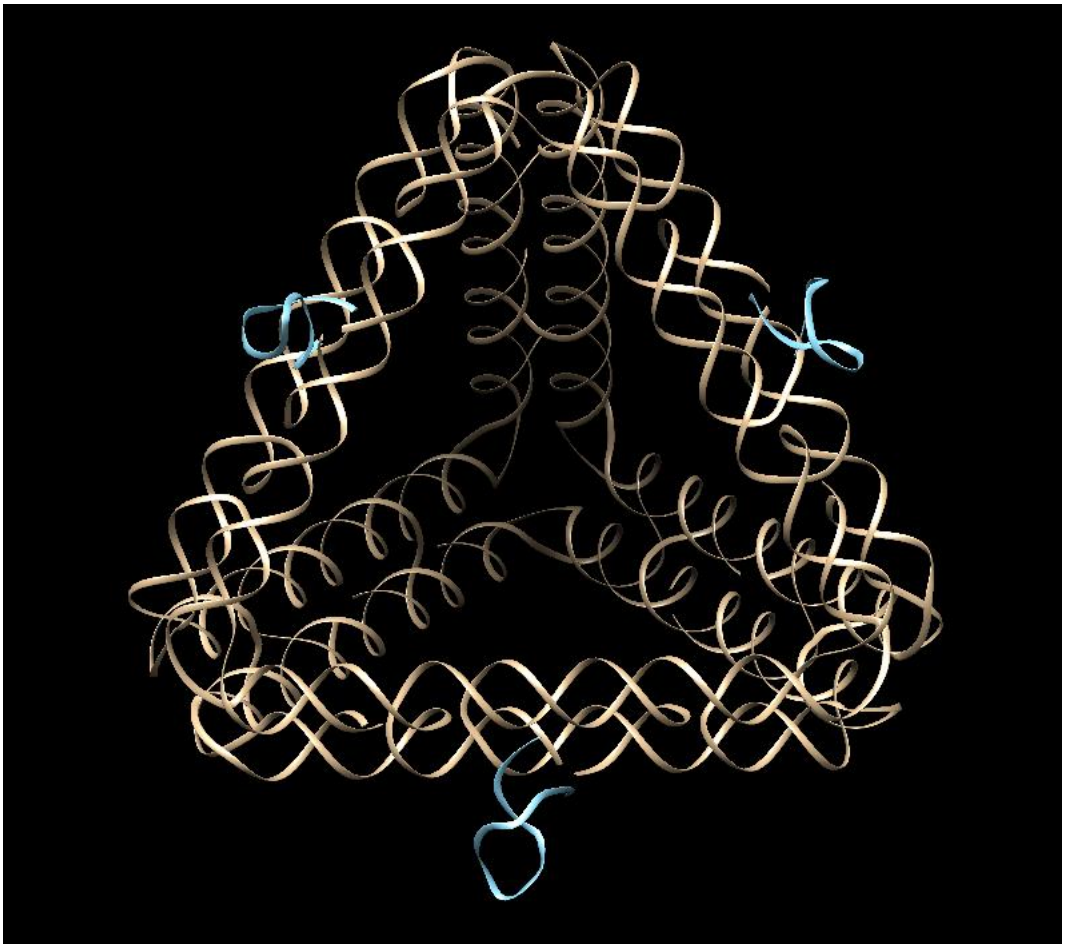

Figure 9: DAEDALUS 42 bp origami unattached aptamer tetrahedron model. This figure serves to provide an illustration and anticipated visualization for the placement of three thrombin 29-mer sequences (unattached from the scaffold).

High-melt 1.5 percent agarose gel electrophoresis revealed our 551 bp thrombin-gBlock sequence could be amplified ssDNA using aPCR (**Fig. 10**). There does appear to be dsDNA and ssDNA biproducts that we believed are produced during the aPCR

process due to non-specific interaction of the forward and reverse primers with the modified thrombin aptamer-template sequence. However, we can acknowledge the thrombin-gBlock aPCR results were consistent enough to proceed with purification.

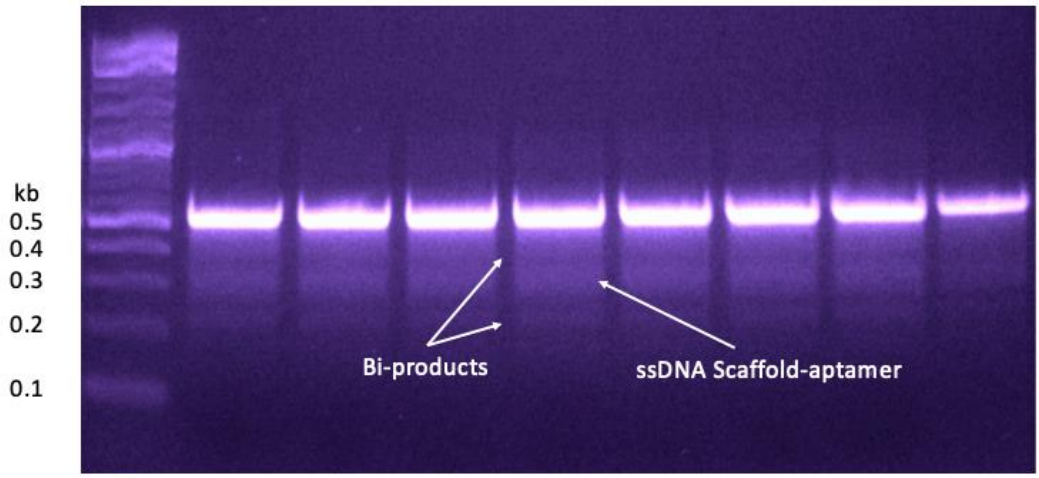

Figure 10: Gel electrophoresis characterization of 551 bp thrombin-gBlock. Post-aPCR thrombin-gBlock shown to migrate dsDNA (top band), dsDNA biproduct (second band), ssDNA (third band) and ssDNA biproduct (last band). Presented on the left, a 1kb plus ladder reference.

After the ssDNA thrombin-gBlock template was purified, we were able to reveal the following (**Fig. 11**): (1) amplified thrombin-gBlock ssDNA with dsDNA and ssDNA bi-products (i.e., 0.4kb band and 0.2kb band), (2) purified thrombin-gBlock dsDNA and ssDNA and (3) purified thrombin-gBlock dsDNA aPCR product. We observed that

purified thrombin-gBlock dsDNA could not express the capability to be used as a template during aPCR. After displaying our purified ssDNA corresponds to the extracted ssDNA thrombin-gBlock, the sample can be prepared for folding.

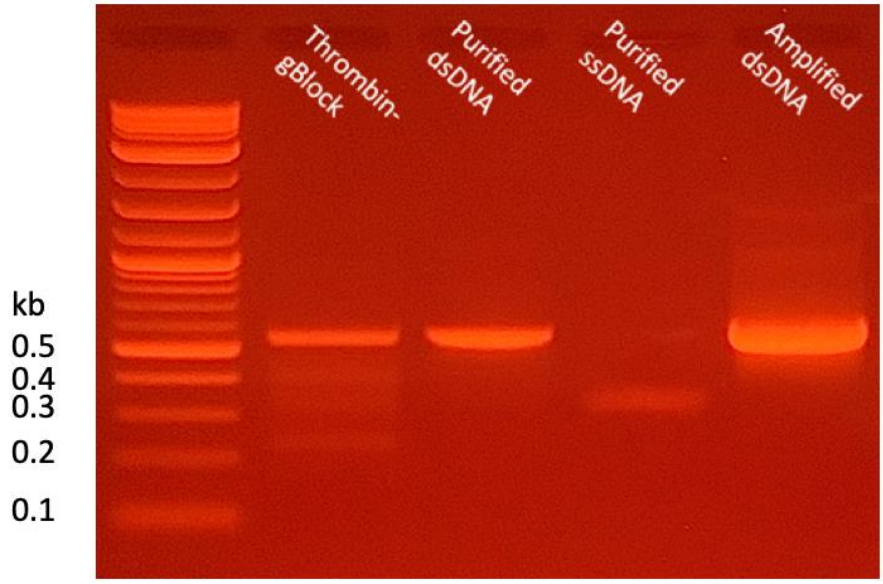

Figure 11: Gel electrophoresis characterization illustrating the migration of various samples. Left to right: 1kb plus ladder, post-aPCR thrombin-gBlock, purified thrombin-gBlock dsDNA, purified thrombin-gBlock ssDNA, amplified thrombin-gBlock dsDNA.

4. Conclusion and Future Work

Herein, we show evidence of a novel method that allows for sequences modified with aptamer sequences to be amplified and prepared for DNA origami folding. This

method should allow for more efficient ways to functionalize DNA nanostructures with various targeting, binding and tracking moieties; however, further steps need to be made that optimize the protocol to minimize amplified bi-products. Lastly, the replacement of thrombin 29-mer with length-varying aptamers and RNA aptamers should be of interest to assess amplification and characterization.

Specific Aim 2: DNA Origami-Aptamer Folding Characterization and Testing Binding Parameters of the Aptamer-Modified DNA Origami.

1. Introduction

By demonstrating the amplification and preparation of our modified sequences, the next step would be to characterize folding and assess the structure's binding capabilities to determine if the aptamer can effectively retain its shape and binding properties. Initially, methodology pertaining to agarose gel characterization and surface plasmon resonance will be discussed followed by their respected results and a discussion with anticipated future work.

2. Methodology

2.1 DNA Origami-Aptamer Folding

Prepared in 50 μL tubes, the folding solution includes 10x folding buffer (TE and $MgCl_2$), 750 nM staple strand mix, 75 nM purified ssDNA scaffold and Ultra-purified distilled water. Using the Bio-Rad T100 Thermal Cycler, the 50 μL folding stock solution will experience the following protocol: 95° C for five minutes, 80° C for five minutes (minus 1° C per cycle) repeated five times, 74° C for 15 minutes (minus 1° C per cycle) repeated 40 times, 30° C for ten seconds (plus 1° C per cycle) repeated five times and

kept at 4° C until further processed. Afterwards, the folded solution will be characterized using gel electrophoresis in a high-melt 1.5 percent agarose.

2.2 Target Binding Agarose Gel Electrophoresis

Characterization process will remain the same with respect to gel and post-aPCR preparation, however, the structures will be introduced to thrombin for 30 minutes before electrophoresis allowing for adequate binding time. With the structure binding to thrombin, we anticipate a higher band compared to thrombin-free sample; this will effectively demonstrate that the aptamer retains its binding properties post-folding. Serving as a negative control, we will amplify and fold an aptamer-free M13 template into the same 3-D tetrahedron structure and introduce it to thrombin.

3. Results and Discussion

3.1 DNA Origami-Aptamer Folding

The M13mp18 and thrombin-gBlock templates were able to fold into 42 bp tetrahedron structures, as signified by the step during electrophoresis (**Fig. 12**). Because of the 1:10 scaffold to staple stand ratio, excess staple stands migrated much further into the gel. Both the purified M13mp18 and thrombin-gBlock ssDNA columns reveal dsDNA biproduct (faint top band), however, we predict this was a result from dsDNA cross-contamination during the extraction or purification stage. Nonetheless, both the M13mp18 and thrombin-gBlock folded tetrahedron structures can progress to assess for target binding.

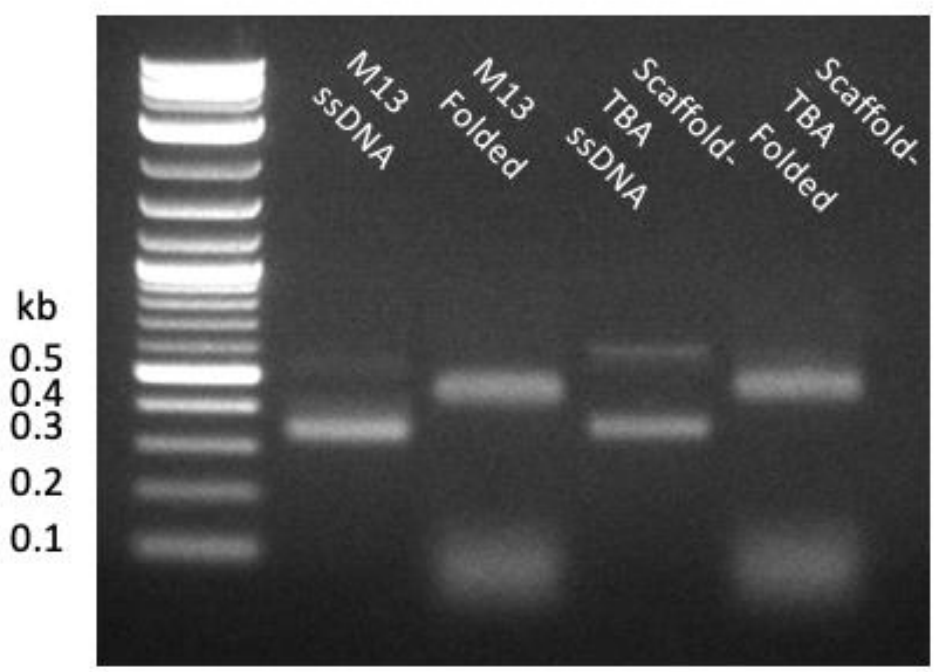

Figure 12: Folding characterization of 42 bp tetrahedron thrombin-gBlock and M13mp18. Left to right: 1kb plus dsDNA ladder, purified M13mp18 ssDNA (lower band), 42 bp tetrahedron M13mp18 and staple strands (lower band), purified thrombin-gBlock ssDNA (lower band) and 42 bp tetrahedron thrombin-gBlock and staple strands (lower band). Within the M13mp18 and thrombin-gBlock ssDNA column, there appears to be dsDNA biproducts.

3.2 Targeting Binding Using Agarose Gel Electrophoresis

Both M13 and thrombin-gBlock ssDNA possess 42 bp tetrahedron folding proficiency indicated by the gradual shift (**Fig. 13**). Introducing both folded structures to

thrombin, only the thrombin-gBlock tetrahedron displays a change in gel migration compared to its thrombin-free control. Not the increase in band size with respect to the folded structures incubated with 10x thrombin. We suggest this was a result of non-specific interaction with thrombin.

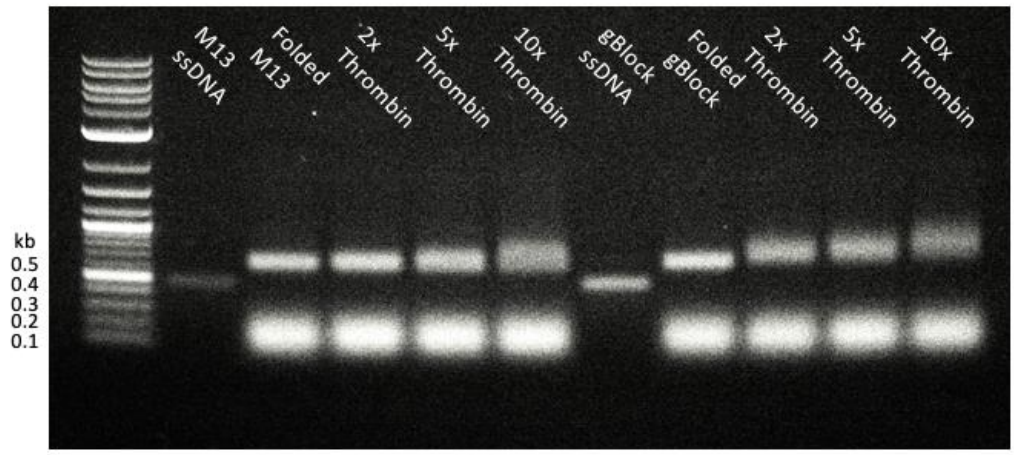

Figure 13: Assessment of thrombin-gBlock and M13 thrombin binding with varying thrombin concentrations. Left to right: ssDNA M13, folded M13 tetrahedron, folded M13 exposed to 2x, 5x and 10x thrombin, ssDNA thrombin-gBlock, folded thrombin-gBlock tetrahedron and folded thrombin-gBlock exposed to 2x, 5x and 10x thrombin. Both the M13 and thrombin-gBlock ssDNA appear to articulate the ability of fold into tetrahedrons as indicated by the gradual shift in comparison to their ssDNA, respectively.

As anticipated, an absent of thrombin binding designated by no shift in the folded M13 with thrombin compared to folded M13 free of thrombin was observed. Compared to folded M13 with and without thrombin, the progressive shift of folded thrombin-gBlock exposed to thrombin indicates the 29-mer retains its binding properties after being folded.

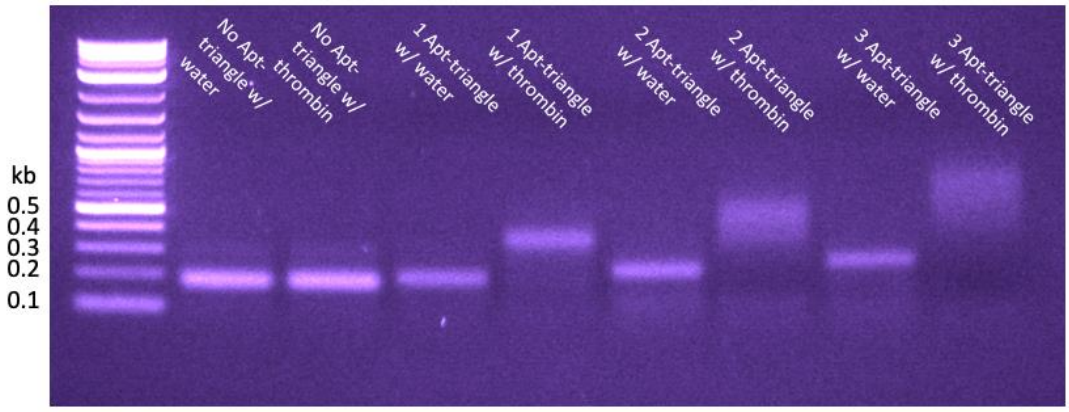

Figure 14: Gel electrophoresis thrombin binding assessment to four triangle origami-aptamer structures. Each structure was exposed to either water (control) or thrombin. As aptamer density increases, the structures experience an increase in molecular weight indicated by the migration.

Here we were able to validate the folding and targeting capabilities associated with the 42 bp triangle displaying our DNA origami-aptamer modification technique

(**Fig. 14**). Where aptamer-free triangles did not exhibit thrombin binding indicated by no observed change in the band migration, the aptamer-triangle did express sufficient binding to thrombin. Additionally, the molecular weight of the folded thrombin-free triangle steadily increases with aptamer density. However, here we observe the impact of non-specific interaction between thrombin and the triangles hybridized with two and three 29-mer. We anticipate this as a result from the thrombin concentration introduced to those structures and with fine tuning, more noticeable bands similar to the one aptamer triangle structure is anticipated.

4. Conclusion and Future Work

By establishing that origami-aptamer folded sequences retain binding properties, our technique of sequence modification may serve as an innovative approach in creating functionalized DNA-based nanoparticles for a wide range of applications including drug delivery, biosensing and theranostics; however, this approach reveals the use of only one well-studied aptamer in the folded sequence. Therefore, assessments should be made towards evaluating the use of different aptamers varying in length and density to observe any change in binding and the DNA origami folding effect.

LIMITATIONS

Herein, we provide proof that one can modify scaffold sequences used to fold DNA origami with the thrombin 29-mer aptamer at precise locations while retaining the ability to effectively target its respected biomarkers. However, we will emphasize some of the limitations and challenges experienced during the process of modification; first, here we demonstrate the use of thrombin 29-mer modified within the sequence and resulting bi-products, allowing one to conclude a lack of optimization and functionalization, however, these results provide a proof of principle that may encourage follow-up studies addressing these problems and attempt to design variety of DNA origami structures with aptamer sequences using this technique; second, we acknowledge the intended application of this approach is to provide a novel method and tool to theoretically target and treat glioblastomas, yet, we did not conduct any studies that display its effectiveness. Nonetheless, while there is literature demonstrating AS1411's effectiveness in treating glioblastomas, follow-up studies using this novel approach of sequence modification may be highly encouraged.

CONCLUSION AND FUTURE WORK

In the past two decades, DNA origami and functional nucleic acid sequences (i.e., aptamers) have gained a lot of traction in research given their unique properties (i.e., biocompatibility, highly modifiable and customizable in shape and size and high binding affinities). DNA origami-aptamer composites may be considered one of the most practical biomaterials for a wide range of biomedical applications including but not limited to therapeutics, diagnostics, theranostics, drug delivery and biosensing. However, there still arises challenges associated with topic, some of which include availability of material and difficulty in *in vitro* synthesis and functionalization of the DNA nanoparticles. By overcoming additional steps required to functionalize DNA origami with aptamers, our strategy provides researchers with a reliable and timely method to efficiently design and characterize origami-aptamer nanoparticles. Here we demonstrated by modeling aptamer "loops" at precise locations on DNA origami structures, one can unify DNA aptamers with the scaffold sequence used in origami folding while retaining the ability to effectively bind to target biomarkers. Yet, this discovery remains in its preliminary stage, therefore, future work with respect to optimization and follow-up studies (i.e., surface plasmon resonance, minimization of bi-products via protocol optimization, assessments on different origami structures, aptamers with different lengths and the use of RNA aptamers) should be performed.

REFERENCES

[1] R. Dahm, "Friedrich Miescher and the Discovery of DNA," *Developmental Biology*, vol. 278, no. 2, pp. 274-88, Feb. 2005, doi: 10.1016/j.ydbio.2004.11.028.

[2] J. M. Heather, and B. Chain, "The Sequence of Sequencers: The History of Sequencing DNA," *Genomics*, vol. 107, no. 1, pp. 1-8, Jan. 2016, doi: 10.1016/j.ygeno.2015.11.003.

[3] A. Tefferi, "Genomics Basics: DNA Structure, Gene Expression, Cloning, Genetic Mapping, and Molecular Tests," *Seminars in Cardiothoracic and Vascular Anesthesia*, vol. 10, no. 4, pp. 282-290, Dec. 2006, doi: 10.1177/1089253206294343.

[4] N. C. Seeman, "Nucleic acid junctions and lattices," *J. Theor. Biol.*, vol. 99, no. 2, pp. 237-247, Nov. 1982, doi: 10.1016/0022-5193(82)90002-9.

[5] Y. Chen, B. Groves, R. A. Muscat, and G. Seelig, "DNA Nanotechnology from the Test Tube to the Cell," *Nature Nanotechnology*, vol. 10, no. 9, pp. 748 -760, Sept. 2015, doi: 10.1038/nnano.2015.195.

[6] P. Rothemund, "Folding DNA to Create Nanoscale Shapes and Patterns," *Nature,* vol. 440, no. 7082, pp. 297-302, Mar. 2006, doi: 10.1038/nature04586.

[7] C. Timm, and C. M. Niemeyer, "Assembly and Purification of Enzyme-Functionalized DNA Origami Structures," *Angewandte Chemie International Edition,* vol. 54, no. 23, pp. 6745 – 50, 2015, doi: 10.1002/anie.201500175.

[8] C. Shen et al., "Site-Specific Surface Functionalization of Gold Nanorods Using DNA Origami Clamps," *Journal of the American Chemical Society*, vol. 138, no. 6, pp. 1764-1767, Feb. 2016, doi: 10.1021/jacs.5b11566.

[9] C. Tuerk, and L. Gold, "Systematic evolution of ligands by exponential enrichment: RNA ligands to bacteriophage T4 DNA polymerase," *Science*, vol. 249, no. 4968, pp. 505-510, Aug. 1990, doi: 10.1126/science.2200121.

[10] S. D. Jayasena, " Aptamers: An Emerging Class of Molecules That Rival Antibodies in Diagnostics," *Clin. Chem.,* vol. 45, no. 9, pp. 1628-1650, Sept. 1999, doi: 10.1093/clinchem/45.9.1628.

[11] R. R. Breaker, and G. F. Joyce, "A DNA enzyme that cleaves RNA," *Chem. & Bio.*, vol. 1, no. 4, pp. 223-229, Dec. 1994, doi: 10.1016/1074-5521(94)90014-0.

[12] A. D. Ellington, and J. W. Szostak, "In vitro selection of RNA molecules that bind specific ligands," *Nature*, vol. 346, no. 6287, pp. 818-822, Aug. 1990, doi: 10.1038/346818a0.

[13] O. C. Farokhzad, S. Jon, A. Khademhosseini, T. T. Tran, D. A. LaVan, and R. Langer, "Nanoparticle-Aptamer Bioconjugates: A New Approach for Targeting Prostate Cancer Cells," *Cancer Res.*, vol. 64, no. 21, pp. 7668-7672, Nov. 2004, doi: 10.1158/0008-5472.CAN-04-2550.

[14] T. C. Chu et al., "Aptamer: Toxin Conjugates that Specifically Target Prostate Tumor Cells," *Cancer Res.*, vol. 66, no. 12, pp. 5989-5992, June 2006, doi: 10.1158/0008-5472.CAN-05-4583.

[15] S. Soundararajan, W. Chen, E. K. Spicer, N. Courtenay-Luck, and D. J. Fernandes, "The Nucleolin Targeting Aptamer AS1411 Destabilizes Bcl-2 Messenger RNA in Human Breast Cancer Cells," *Cancer Res.*, vol. 68, no. 7, pp. 2358-2365, Apr. 2008, doi: 10.1158/0008-5472.CAN-07-5723.

[16] W. Li, T. Bing, J. Wei, Z. Chen, D. Shangguan, and J. Fang," Cell-SELEX-based selection of aptamers that recognize distinct targets on metastatic colorectal cancer cells," *Biomaterials*, vol. 35, no. 25, pp. 6998-7007, Aug. 2014, doi: 10.1016/j.biomaterials.2014.04.112.

[17] X. Pang et al., "Bioapplications of Cell-SELEX-Generated Aptamers in Cancer Diagnostics, Therapeutics, Theranostics and Biomarker Discovery: A Comprehensive Review," *Cancers*, vol. 10, no. 2, pp. 47, Feb. 2018, doi: 10.3390/cancers10020047.

[18] Z. Liu, "Novel HER2 Aptamer Selectively Delivers Cytotoxic Drug to HER2-Positive Breast Cancer Cells in Vitro," *J. Transl Med.*, vol. 10, no. 1, pp. 148, July 2012, doi: 10.1186/1479-5876-10-148.

[19] J. G. Bruno, "A Review of Therapeutic Aptamer Conjugates with Emphasis on New Approaches," *Pharmaceuticals*, vol. 6, no. 3, pp. 340-357, Mar. 2013, doi: 10.3390/ph6030340.

[20] L. Yang, "Photothermal Therapeutic Response of Cancer Cells to Aptamer–Gold Nanoparticle-Hybridized Graphene Oxide under NIR Illumination," *ACS Appl. Mater. Interfaces*, vol. 7, no. 9, pp. 5097-5106, Mar. 2015, doi: 10.1021/am508117e.

[21] J. K. Herr, J. E. Smith, C. D. Medley, D. Shangguan, and W. Tan, "Aptamer-Conjugated Nanoparticles for Selective Collection and Detection of Cancer Cells," *Anal. Chem.*, vol. 78, no. 9, pp. 2918-2924, May 2006, doi: 10.1021/ac052015r.

[22] D. Shangguan Z. C. Cao, Y. Li, and W. Tan, "Aptamers Evolved from Cultured Cancer Cells Reveal Molecular Differences of Cancer Cells in Patient Samples," *Clin. Chem.*, vol. 53, no. 6, pp. 1153-1155, June 2007, doi: 10.1373/clinchem.2006.083246.

[23] C. D. Medley, J. E. Smith, Z. Tang, Y. Wu, S. Bamrungsap, and W. Tan, "Gold Nanoparticle-Based Colorimetric Assay for the Direct Detection of Cancerous Cells," *Anal. Chem.*, vol. 80, no. 4, pp. 1067-1072, Feb. 2008, doi: 10.1021/ac702037y.

[24] V. Bagalkot et al., "Quantum Dot−Aptamer Conjugates for Synchronous Cancer Imaging, Therapy, and Sensing of Drug Delivery Based on Bi-Fluorescence Resonance Energy Transfer," *Nano Lett.*, vol. 7, no. 10, pp. 3065-3070, Oct. 2007, doi: 10.1021/nl071546n.

[25] S. Yang et al., "Oligonucleotide Aptamer-Mediated Precision Therapy of Hematological Malignancies," *Molecular Therapy - Nucleic Acids*, vol. 13, pp. 164-175, Dec. 2018, doi: 10.1016/j.omtn.2018.08.023.

[26] M. Yan, M. Schwaederle, D. Arguello, S. Z. Millis, Z. Gatalica, and R. Kurzrock, "HER2 Expression Status in Diverse Cancers: Review of Results from 37,992 Patients," *Cancer Metastasis Rev*, vol. 34, no. 1, pp. 157-164, Mar. 2015, doi: 10.1007/s10555-015-9552-6.

[27] C. R. Ireson, and L. R. Kelland, "Discovery and Development of Anticancer Aptamers," *Mol. Cancer Ther.*, vol. 5, no. 12, pp. 2957-2962, Dec. 2006, doi: 10.1158/1535-7163.MCT-06-0172.

[28] C. M. Berger, X. Gaume, and P. Bouvet, "The Roles of Nucleolin Subcellular Localization in Cancer," *Biochimie*, vol. 113, pp. 78-85, June 2015, doi: 10.1016/j.biochi.2015.03.023.

[29] Z. Chen, and X. Xu, "Roles of Nucleolin," *Saudi Med. J.*, vol. 37, no. 12, pp. 1312-1318, Dec. 2016, doi: 10.15537/smj.2016.12.15972.

[30] M. Delač, H. Motaln, H. Ulrich, and T. Lah, "Aptamer for Imaging and Therapeutic Targeting of Brain Tumor Glioblastoma," *Cytometry Part A*, vol. 87, no. 9, pp. 806-816, 2015, doi: 10.1002/cyto.a.22715.

[31] Z. Luo et al., "Precise Glioblastoma Targeting by AS1411 Aptamer-Functionalized Poly (l-γ-Glutamylglutamine)–Paclitaxel Nanoconjugates," *Journal of Colloid and Interface Science*, vol. 490, pp. 783-96, Mar. 2017, doi: 10.1016/j.jcis.2016.12.004.

[32] R. Yazdian-Robati et al., "Therapeutic Applications of AS1411 Aptamer, an Update Review," *International Journal of Biological Macromolecules*, vol. 155, pp. 1420-31, July 2020, doi: 10.1016/j.ijbiomac.2019.11.118.

[33] E. M. Reyes-Reyes, F. R. Šalipur, M. Shams, M. K. Forsthoefel, and P. J. Bates, "Mechanistic Studies of Anticancer Aptamer AS1411 Reveal a Novel Role for Nucleolin in Regulating Rac1 Activation," *Molecular Oncology*, vol. 9, no. 7, pp. 1392-1405, Aug. 2015, doi: 10.1016/j.molonc.2015.03.012.

[34] E. M. Reyes-Reyes, Y. Teng, and P. J. Bates, "A New Paradigm for Aptamer Therapeutic AS1411 Action: Uptake by Macropinocytosis and Its Stimulation by a Nucleolin-Dependent Mechanism," *Cancer Res.*, vol. 70, no. 21, pp. 8617-8629, Nov. 2010, doi: 10.1158/0008-5472.CAN-10-0920.

[35] Q. Jiang et al., "DNA Origami as a Carrier for Circumvention of Drug Resistance," *J. Am. Chem. Soc.*, vol. 134, no. 32, pp. 13396-403, Aug. 2012, doi: 10.1021/ja304263n.

[36] Y. X. Zhao, A. Shaw, X. Zeng, E. Benson, A. M. Nyström, and B. Högberg, "DNA Origami Delivery System for Cancer Therapy with Tunable Release Properties," *ACS Nano*, vol. 6, no. 10, pp. 8684-91, Oct. 2012, doi: 10.1021/nn3022662.

[37] Q. Zhang et al., "DNA Origami as an In Vivo Drug Delivery Vehicle for Cancer Therapy," *ACS Nano*, vol. 8, no. 7, pp. 6633-43, July 2014, doi: 10.1021/nn502058j.

[38] A. Udomprasert, and T. Kangsamaksin, "DNA Origami Applications in Cancer Therapy," *Cancer Sci.*, vol. 108, no. 8, pp. 1535-43, 2017, doi: 10.1111/cas.13290.

[39] X. Zhuang et al., "A Photosensitizer-Loaded DNA Origami Nanosystem for Photodynamic Therapy," *ACS Nano*, vol. 10, no. 3, pp. 3486-95, Mar. 2016, doi: 10.1021/acsnano.5b07671.

[40] Q. Jiang et al., "A Self-Assembled DNA Origami-Gold Nanorod Complex for Cancer Theranostics," *Small*, vol. 11, no. 38, pp. 5134-41, 2015, doi: 10.1002/smll.201501266.

[41] R. Veneziano et al., "Designer Nanoscale DNA Assemblies Programmed from the Top Down," *Science*, vol. 352, no. 6293, pp. 1534, June 2016, doi: 10.1126/science.aaf4388.

[42] P. Wang, T. A. Meyer, V. Pan, P. K. Dutta, and Y. Ke, "The Beauty and Utility of DNA Origami," *Chem*, vol. 2, no. 3, pp. 359-82, Mar. 2017, doi: 10.1016/j.chempr.2017.02.009.

[43] N. P. Truong, M. R. Whittaker, C. W. Mak, and T. P. Davis, "The Importance of Nanoparticle Shape in Cancer Drug Delivery," *Expert Opinion on Drug Delivery*, vol. 12, no. 1, pp. 129-142, Jan. 2015, doi: 10.1517/17425247.2014.950564.

[44] T. J. Dougherty et al., “Photodynamic Therapy,” *J. Natl. Cancer Inst.*, vol. 90, no. 12, pp. 889-905, June 1998, doi: 10.1093/jnci/90.12.889.

[45] D. E. J. G. J. Dolmans, D. Fukumura, and R. K. Jain, “Photodynamic Therapy for Cancer,” *Nat. Rev. Cancer*, vol. 3, no. 5, pp. 380-387, May 2003, doi: 10.1038/nrc1071.

[46] P. Agostinis et al., “Photodynamic Therapy of Cancer: An Update,” *CA: A Cancer Journal for Clinicians*, vol. 61, no. 4, pp. 250-281, 2011, doi: 10.3322/caac.20114.

[47] B. Saccà, and C. M. Niemeyer, “Functionalization of DNA Nanostructures with Proteins,” *Chem. Soc. Rev*, vol. 40, no. 12, pp. 5910-5921, 2011, doi: 10.1039/C1CS15212B.

[48] T. L. Doane, R. Alam, and M. M. Maye, “Functionalization of Quantum Rods with Oligonucleotides for Programmable Assembly with DNA Origami,” *Nanoscale*, vol. 7, no. 7, pp. 2883-2888, 2015, doi: 10.1039/C4NR07662A.

[49] M. Godonoga et al., “A DNA Aptamer Recognising a Malaria Protein Biomarker Can Function as Part of a DNA Origami Assembly,” *Scientific Reports*, vol. 6, no. 1, pp. 21266, Feb. 2016, doi: 10.1038/srep21266.

[50] P. Wang, T. A. Meyer, V. Pan, P. K. Dutta, and Y. Ke, “The Beauty and Utility of DNA Origami,” *Chem*, vol. 2, no. 3, pp. 359-82, Mar. 2017, doi: 10.1016/j.chempr.2017.02.009.

[51] Y. Tian, Y. Huang, P. Gao, and T. Chen, “Nucleus-Targeted DNA Tetrahedron as a Nanocarrier of Metal Complexes for Enhanced Glioma Therapy,” *Chemical Communications*, vol. 54, no. 68, pp. 9394-97, 2018, doi: 10.1039/C8CC04021D.

[52] K. Liu, C. Xu, and J. Liu, “Regulation of Cell Binding and Entry by DNA Origami Mediated Spatial Distribution of Aptamers,” *Journal of Materials Chemistry B*, vol. 8, no. 31, pp. 6802-9, 2020, doi: 10.1039/D0TB00663G.

[53] Q. Pan et al., “Aptamer Functionalized DNA Origami for Targeted Codelivery of Antisense Oligonucleotides and Doxorubicin to Enhance Therapy in Drug-Resistant Cancer Cells,” *ACS Applied Materials & Interfaces*, vol. 12, no. 1, pp. 400-9, Jan. 2020, doi: 10.1021/acsami.9b20707.

[54] M. Cao et al., “Multivalent Aptamer-Modified DNA Origami as Drug Delivery System for Targeted Cancer Therapy,” *Chemical Research in Chinese Universities*, vol. 36, no. 2, pp. 254-60, Apr. 2020, doi: 10.1007/s40242019-9273-4.

[55] S. Zhao et al., "A DNA Origami-Based Aptamer Nanoarray for Potent and Reversible Anticoagulation in Hemodialysis," *Nat. Comm.*, vol. 12, no. 1, pp. 358, Jan. 2021, doi: 10.1038/s41467-020-20638-7.

[56] J. Nangreave, D. Han, Y. Liu, and H. Yan, "DNA Origami: A History and Current Perspective," *Curr. Opin. Chem. Biol.*, vol. 14, no. 5, pp. 608-615, Oct. 2010, doi: 10.1016/j.cbpa.2010.06.182.

[57] T. Tørring, N. V. Voigt, J. Nangreave, H. Yan, and K. V. Gothelf, "DNA Origami: A Quantum Leap for Self-Assembly of Complex Structures," *Chemical Society Reviews*, vol. 40, no. 12, pp. 5636-5646, 2011, doi: 10.1039/C1CS15057J.

[58] Y. Sakai, M. S. Islam, M. Adamiak, S. C. Shiu, J. A. Tanner, and J. G. Heddle, "DNA Aptamers for the Functionalisation of DNA Origami Nanostructures," *Genes*, vol. 9, no. 12, pp. 571, Dec. 2018, doi: 10.3390/genes9120571.

[59] D. Balakrishnan, G. D. Wilkens, and J. G. Heddle, "Delivering DNA Origami to Cells," *Nanomedicine*, vol. 14, no. 7, pp. 911-925, Apr. 2019, doi: 10.2217/nnm-2018-0440.

[60] S. Williams, K. Lund, C. Lin, P. Wonka, S. Lindsay, and H. Yan, "Tiamat: A Three-Dimensional Editing Tool for Complex DNA Structures," vol. 5347, pp.90–101, 2008, doi: 10.1007/978-3-642-03076-58.

[61] R. Veneziano, T. R. Shepherd, S. Ratanalert, L. Bellou, C. Tao, and M. Bathe, "In Vitro Synthesis of Gene-Length Single-Stranded DNA," *Scientific Reports*, vol. 8, no. 1, pp. 6548, Apr. 2018, doi: 10.1038/s41598-018-24677-5.

BIOGRAPHY

Bailey Jacob O'Shea graduated from Great Bridge High School, Chesapeake, Virginia, in 2016. He received his Bachelor of Science from George Mason University in 2020 and shortly afterwards received a Master of Science in Bioengineering from George Mason University in 2021.